Sensorless Direct Torque Control of Electrical Drives Based on Flux Estimator Using Integrator with DC-offset Correction Loop

Gheorghe Daniel Andreescu and Adrian Popa

Abstract—**This paper develops a flux-linkage estimator using voltage model in stator reference based on an improved integrator with DC-offset PI-correction loop having the reference flux magnitude in the correction error. The DC-offset and drift from acquisition channels and the flux-vector initial error are canceled. A phase locked-loop state estimator extracts the speed and position from the estimated rotor flux. This robust solution can be applied in all AC drives with sinusoidal flux distribution in wide speed range, including sensorless control. A sensorless DTC is investigated for both PMSM and IM drives. Simulation results for PMSM drive and also experimental results for IM drive prove high-dynamic performances in large speed range step reversal, for zero to rated load-torque step.**

Index Terms—**Direct torque control, flux estimator, integrator with DC-offset correction, sensorless control**

I. Introduction

ADVANCED control of electrical drives requires a decoupling control of electromagnetic torque and flux as for field oriented vector control (FOC) or direct torque and flux control (DTC) [1], [2]. DTC provides a very quick torque response (few ms) with good robustness to parameter variations and disturbances. Its implementation is simple, without complex field-orientation blocks.

Two main strategies are used for DTC of AC drives:
1) voltage-vector selection using a switching table [1]-[5],
2) space-vector modulation (SVM) [6]-[8].

The first strategy is commonly commercialized for industrial applications because it is very simple in concept and implementation. This is based on an independent hysteresis control of torque and flux, and an optimal switching table to directly command the voltage source inverter (VSI), without complex PWM techniques and without rotational operators. The main drawback is the high current/torque ripple in steady state operation, especially in low speed range. To obtain good performances high sampling rates are required ($h = 25$ μs) [4], that constitute a high computational burden with standard microcontroller.

The second strategy SVM provides a substantial reduction of current and torque ripples but increases the computational effort.

The crucial problem of DTC and FOC for sensorless control of AC drives is the accurate dynamic estimation of the stator flux vector in wide speed range using only the terminal variables: currents, voltages. The electromagnetic torque can be easily computed from the estimated stator flux vector and the measured stator current vector.

This paper is focused to develop a robust flux estimator for all vector-controlled AC drives with sinusoidal flux distribution, including sensorless control. This is based on an improved integrator using the voltage model with a DC-offset PI-correction loop. The correction error utilizes the reference flux magnitude that forces the flux vector onto a circular trajectory. The speed and position are extracted from the rotor flux vector using a phase locked-loop (PLL) state estimator. As application example, a sensorless DTC is investigated based on this estimation technique, for both PMSM – by simulation, and IM – by experiment. The proposed solution is considered as an improved solution compared with [9] and can be applied in sensorless DTC.

II. Flux-Linkage Estimators

The flux-linkage estimation can be obtained using current models (EI) or voltage models (EU) having different sensitivities regarding model parameter errors [10]-[13].

The EI flux estimators severely depend on magnetic parameters (inductances, permanent magnet of PMSM) and use the measured stator currents, and additionally the electrical angle or speed. They are recommended at low speed, even zero speed.

On the other hand, the EU^s flux estimator in stator reference (the superscript "s" refers to the reference frame) (1) is generally applicable to a lot of machines as IM, PMSM, synchronous reluctance motor, etc.

$$\dot{\boldsymbol{\lambda}} = \mathbf{e} = \mathbf{u}_s - R_s \mathbf{i}_s, \quad \boldsymbol{\lambda}(0) = \boldsymbol{\lambda}_0, \tag{1}$$

where: $\boldsymbol{\lambda}$ – flux-linkage vector, $\boldsymbol{\lambda}_0$ – initial flux value, $\mathbf{e}$ – electromotive force (emf) vector, $\mathbf{i}_s$ – stator current vector, $\mathbf{u}_s$ – stator voltage vector, R_s – stator resistance. The superscript "$\cdot$" refers to the derivative operator.

A. Emf Vector Estimation

The estimation of the emf vector $\hat{\mathbf{e}}$ uses the measured $\mathbf{i}_s$, estimated $\hat{\mathbf{u}}_s$ and estimated $\hat{R}_s$, where the superscript "$\hat{}$" refers to estimated values.

$$\hat{\mathbf{e}} = \hat{\mathbf{u}}_s - \hat{R}_s \mathbf{i}_s. \tag{2}$$

At very low speed, the voltage-drop in inverter can be higher than the emf voltage, constituting a dominant disturbance. To obtain an accurate $\hat{\mathbf{u}}_s$ estimation, a VSI model is used where the power devices are modeled by an

Manuscript received July 16, 2002; revised April 9, 2003.

G. D. Andreescu is with the Automation and Industrial Informatics Department, University "Politehnica" of Timisoara, Timisoara, RO-1900 Romania, (e-mail: dandre@aut.utt.ro).

A. Popa is with the Siemens VDO Automotive, Timisoara, RO-1900, Romania, (e-mail: adrian.popa@siemens.com).

Publisher Item Identifier S 1682-0053(03)0168

average threshold voltage u_{th}, an average differential resistance r_d and the VSI dead time (τ_{VSI}) [14]. Typically for IGBT: $u_{th} = 1-2$ V, $r_d = 0.02-0.05$ Ohm, $\tau_{VSI} = 0.5-2$ μs.

The $\hat{\mathbf{u}}_s$ estimation can be reconstructed from the inverter switching binary state $(S_a, S_b, S_c) \in \{0,1\}$ and the measured DC link-voltage (V_{dc}) (3), with the correction (4). For DTC with voltage-vector selection using a switching table, the VSI applies a full voltage vector in a sampling period h, and thus the dead time compensation is as in (4).

$$\hat{\mathbf{u}}_s = \hat{V}_{dc}(2S_a - S_b - S_c)/3 + \mathrm{j}\hat{V}_{dc}(S_b - S_c)/\sqrt{3}, \quad (3)$$

$$\hat{V}_{dc} = (V_{dc} - 2u_{th})(1 - \tau_{VSI}/h), \quad (4)$$

$$\hat{R}_s = \hat{R}_{sp} + 2r_d + R_f. \quad (5)$$

The equivalent stator-resistance estimation $\hat{R}_s$ (5) contains the stator phase resistance $\hat{R}_{sp}$, the power device resistance r_d and the feeder resistance R_f. The resistance $\hat{R}_{sp}$ is the most important and it linearly depends by the stator temperature. The $\hat{R}_s$ estimation could use low cost sensors to measure the stator temperature, or usually, real-time parameter identification algorithms [14]-[17]. Really, to allow a correct flux estimation, especially at low speed, the equivalent resistance $\hat{R}_s$ is required to be correct adapted.

B. Pure Integrator Drawbacks

The EU[s] flux estimator seems to be a very attractive solution for sensorless control of AC drives. Unfortunately, the EU[s] flux estimator is obtained using a pure integrator (1) with the following drawbacks pointed out especially at low speed [14]-[19]:

- DC-drift components coming from the analog to digital converters (ADC) of current or voltage transducers lead the pure integrator into saturation limit.
- An incorrect initial value of the integrator $\boldsymbol{\lambda}_0$ produces a constant DC-offset at the integrator output.
- The DC-offset can be generated by rapid change in harmonic input signals, e.g., in speed reversal.

C. Flux-Linkage Estimators Using Voltage-Model

Recently, a wide diversity of sensorless flux-linkage estimators using voltage-model with equivalent integrators were investigated. All of them tend to have the same frequency behavior as the pure integrator: $H_I = (1/\omega)\mathrm{e}^{-\mathrm{j}\pi/2}$, where ω is the input frequency. The main problems are the estimation accuracy at low speed, and to obtain high-estimation bandwidth in fast transient operations. Certain equivalent integrator solutions are discussed below.

1) First Order Low-pass Filter

First order low-pass filter (LPF1) with a large time constant is used for $\omega > 4\omega_c$, where ω – stator frequency, ω_c – cut-off filter frequency, usually $\omega_c = 0.5-2$ Hz. The DC-offset is not fully avoided and it has a very slow decay. At low speed, important phase and amplitude errors occur in estimation. A narrow speed range 1:10 is obtained.

2) Programmable-Cascade Adaptive Low-Pass Filter

Programmable-cascade adaptive low-pass filter (PC-ALPF1n) with adaptive time constant τ and gain g depending on the estimated flux frequency $\hat{\omega}$ is proposed in [18]; e.g., if $n = 2$, then $\tau = 1/\hat{\omega}$, $g = 2/\hat{\omega}$, DC-offset amplification $A = 2/\hat{\omega}$. The cascade has an equivalent short time constant and thus the DC-offset has a fast decay. A large speed range 1:100 is obtained in practice. On the other hand, at low frequency, if $\hat{R}_s$ is not adequately identified in real-time, large estimation errors occur. All solutions based on the emf estimation have this drawback. PC-ALPF1n phase is a sum of ALPF1 component phases $\hat{\omega}$ depending. Therefore, the estimated flux phase presents a cumulative effect of errors from ALPF1 phase components. The PC-ALPF1n is not robust to $\hat{\omega}$ deviation.

3) Closed-loop Integrator Plus Adaptive LPF1

Closed-loop integrator plus adaptive LPF1 (I+ALPF1) with adaptive time constant and gain depending on the estimated flux frequency $\hat{\omega}$ is an alternative challenge solution for PC-ALPF1n. The closed loop transfer function of the new equivalent integrator for $n = 2$ (can be generalized) is $H(s) = C(s+\omega_2)/(s+\omega_1)^2$, where $\omega_2 = \hat{\omega}$, $\omega_1 = \hat{\omega}/2.414$ and $C = 0.828$. Therefore, the phase is –π/2, but $A = 4.83/\hat{\omega}$. The I+ALPF1 phase is the difference between the $H(s)$ component phases and therefore, this estimator is more robust to $\hat{\omega}$ deviation if $\omega > \hat{\omega}$, in comparison with the PC-ALPF1n.

4) Modified Integrator with Adaptive Compensation

This solution is proposed in [19] for applications with variable flux-linkage magnitude, in 1:100 speed range, including sensorless control. In the adaptive mechanism, a PI compensator modifies the flux magnitude on the feedback to force the stator flux onto a circular trajectory. Intensive computation as Cartesian to polar and polar to Cartesian operators is used for each axis reference. While the flux is correctly estimated in steady state, there are large estimation errors during fast transient operations and also at start-up [14].

III. Integrator with DC-Offset Correction Loop

A. Flux-Linkage Estimation

In the typical case of the flux control with constant magnitude, the trajectory of the harmonic flux-linkage vector $\boldsymbol{\lambda}_h$ in stator reference is a circle origin centered. If a DC-offset vector $\boldsymbol{\lambda}_{dc}$ appears, the trajectory of the resulted flux vector $\boldsymbol{\lambda} = \boldsymbol{\lambda}_h + \boldsymbol{\lambda}_{dc}$ is also a circle but with the origin drifted by $\boldsymbol{\lambda}_{dc}$ [2], [7], [14], [17]. Thus, the estimation $\hat{\boldsymbol{\lambda}}_{dc} = \hat{\boldsymbol{\lambda}} - \hat{\boldsymbol{\lambda}}_h$ gives information on the circle center eccentricity. The DC-offset vector $\boldsymbol{\lambda}_{dc}$ at the integrator output is the effect of the input DC-drift vector $\mathbf{e}_{dc}$, or of errors in initial flux $\boldsymbol{\lambda}_0$.

A closed-loop integrator with a PI correction for DC-offset is developed for flux-linkage estimation (Fig. 1).

In order to cancel $\boldsymbol{\lambda}_{dc}$, a feedback correction error is used based on the estimated DC-offset flux vector $\hat{\boldsymbol{\lambda}}_{dc}$ (6). The estimated flux $\hat{\boldsymbol{\lambda}}$ is obtained at the integrator output, and $\hat{\boldsymbol{\lambda}}_h$ is approximated by the estimated reference flux $\boldsymbol{\lambda}^*$ having the amplitude λ^* and the same phase $\hat{\theta}_\lambda$ as $\hat{\boldsymbol{\lambda}}$ vector [14], [16], [17]. The superscript " * " refers to reference value.

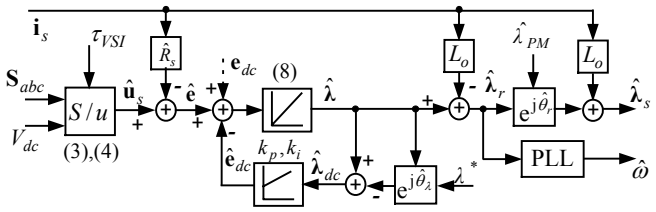

Fig. 1. Flux estimator $\hat{\boldsymbol{\lambda}}$ using improved closed-loop integrator with DC-offset PI correction for all AC machines with sinusoidal flux distribution; $\hat{\boldsymbol{\lambda}}_s$, $\hat{\boldsymbol{\lambda}}_r$ estimations - for PMSM.

$$\hat{\boldsymbol{\lambda}}_{dc} = \hat{\boldsymbol{\lambda}} - \boldsymbol{\lambda}^*, \quad \hat{\boldsymbol{\lambda}} = \hat{\lambda}\, e^{j\hat{\theta}_\lambda}, \quad \boldsymbol{\lambda}^* = \lambda^* e^{j\hat{\theta}_\lambda}, \text{ or} \tag{6}$$

$$\hat{\boldsymbol{\lambda}}_{dc} = (\hat{\lambda}_\alpha + j\hat{\lambda}_\beta)\,(1 - \frac{\lambda^*}{\hat{\lambda}}), \quad \hat{\lambda} = \sqrt{\hat{\lambda}_\alpha^2 + \hat{\lambda}_\beta^2}\ . \tag{7}$$

The disturbance compensation uses a PI compensator with parameters k_p, k_i that estimates the DC-drift input vector $\hat{\mathbf{e}}_{dc} = (k_p + k_i/s)\hat{\boldsymbol{\lambda}}_{dc}$. The closed-loop flux estimation is given by

$$\hat{\boldsymbol{\lambda}}^\bullet = \hat{\mathbf{e}} - \hat{\boldsymbol{\lambda}}\,(1 - \frac{\lambda^*}{\hat{\lambda}})(k_p + \frac{k_i}{s})\ . \tag{8}$$

In essence, the correction term applied to the PI compensator is the difference between the estimated flux and the estimated reference flux. This procedure forces the flux vector onto a circular trajectory with asymptotic phase convergence. The DC-estimation $\hat{\mathbf{e}}_{dc}$ is memorized by the PI integral component and it totally cancels the DC-drift. The flux estimator works as a pure integrator with zero-lag and high-dynamics. The proposed flux estimator can be applied for sensorless control of AC drives with sinusoidal flux distribution, in wide speed range, e.g., PMSM, IM, etc.

B. PI Compensator Design

The equivalent transfer function of the closed-loop integrator with PI compensator is given by

$$\mathbf{H}(s) = \frac{\hat{\boldsymbol{\lambda}}}{\hat{\mathbf{e}}} = \frac{s}{s^2 + k_p s + k_i}\,. \tag{9}$$

This expression points out that the structure from Fig. 1 cancels the DC-offset; if $\hat{\mathbf{e}} = \mathbf{e}_{dc}$ then $\hat{\boldsymbol{\lambda}} = \mathbf{0}$.

The DC-drift input vector $\mathbf{e}_{dc}$, produced by ADC offset and/or by error in initial flux $\hat{\boldsymbol{\lambda}}_0$, has *very slow variations in practice*. The PI integral component memorizes the $\hat{\mathbf{e}}_{dc}$ estimation. Therefore, $\hat{\lambda} = \lambda^*$ in (8), the loop is open, the structure works as a pure integrator with high bandwidth.

If $\hat{\lambda} \neq \lambda^*$, the loop correction is active and the equivalent structure is given by (9). To have a quick asymptotic estimation for $\hat{\mathbf{e}}_{dc}$, we recommends to chose for the PI compensator design the following values:

$$\begin{aligned} &k_i = \omega_0{}^2,\ \omega_0 = \omega_{\min}/d,\ d \in [4,8] \\ &k_p = 2\xi\omega_0,\ \xi \in [0.5,1] \end{aligned}, \tag{10}$$

where $\omega_{\min}$ is the minimum input frequency. In this condition, the phase of the equivalent integrator (9) tends to $-\pi/2$, and practically the phase error is very small if $\omega >> \omega_0$, even in presence of R_s identification error.

C. Rotor Flux Estimation

To extract the mechanical speed and position, the current model EI^s is used to obtain estimated rotor flux $\hat{\boldsymbol{\lambda}}_r(\hat{\boldsymbol{\lambda}}, \mathbf{i}_s)$.

For PMSM with surface-mounted magnets, the PM rotor flux estimation $\hat{\boldsymbol{\lambda}}_r$ is given by (11), where L_o – stator inductance, $\hat{\theta}_r$ – rotor flux phase, and $\hat{\lambda}_r = \hat{\lambda}_{PM}$ – PM-flux.

$$\hat{\boldsymbol{\lambda}}_r = \hat{\boldsymbol{\lambda}} - L_o \mathbf{i}_s,\ \hat{\boldsymbol{\lambda}}_r = \hat{\lambda}_r e^{j\hat{\theta}_r}\,. \tag{11}$$

For IM, the rotor flux vector $\hat{\boldsymbol{\lambda}}_r$ in stator reference is

$$\hat{\boldsymbol{\lambda}}_r = (\hat{\boldsymbol{\lambda}} - \sigma L_s \mathbf{i}_s) L_r / L_m\,, \tag{12}$$

where L_s, L_r, L_m are stator, rotor and mutual inductances, respectively, and $\sigma = 1 - L_m^2 / L_r L_s$.

D. Flux-Linkage Magnitude Correction

Only if errors appear in $\hat{R}_s$ real-time identification, the PI correction-loop must compensate a harmonic error $\Delta R_s \mathbf{i}_s$ by adjusting the estimated stator flux magnitude $\hat{\lambda}$ that fails. On the other hand, in the conditions (10), the stator flux phase estimation $\hat{\theta}_\lambda$ has minor errors [9]. Thus, for accurate stator flux estimation, a second estimation $\hat{\boldsymbol{\lambda}}_s$ is used.

For PMSM, that is:

$$\hat{\boldsymbol{\lambda}}_s = \hat{\lambda}_{PM} e^{j\hat{\theta}_r} + L_o \mathbf{i}_s\,. \tag{13}$$

$\hat{\lambda}_{PM}(t_r)$ depends on the rotor temperature t_r that can be estimated from the measured or estimated stator temperature t_s. In first approximation, $t_r = t_s k/(1 + sT_t)$, where T_t – thermal time constant in range of minutes and k – gain near to 1. For ferrites, λ_{PM} linearly decreases with t_r, i.e., –10% per 50°C.

On the other hand, if $\hat{R}_s(t_s)$ is correctly identified in real time, then $\hat{\lambda}_{PM}(t_r) = \lambda_{PM0} + \Delta\lambda_{PM}$ with

$$\Delta\lambda_{PM} = -\frac{\lambda_{PM0}}{R_{s0}} \Delta\hat{R}_s \frac{k_\lambda}{1 + sT_t}\,, \tag{14}$$

where $\lambda_{PM0} = \lambda_{PM}(t_r = t_{r0})$, $R_{s0} = R_s(t_s = t_{s0})$, $\Delta\hat{R}_s = \hat{R}_s - R_{s0}$, t_{s0}, t_{r0} – initial stator and rotor temperatures, respectively.

For IM, the rotor resistance $\hat{R}_r(t_r)$ can be estimated following the same idea: $\hat{R}_r(t_r) = R_{r0} + \Delta R_r$ with

$$\Delta R_r = \frac{R_{r0}}{R_{s0}} \Delta\hat{R}_s \frac{k_R}{1 + sT_t}\,, \tag{15}$$

where $R_{r0} = R_r(t_r = t_{r0})$.

The electromagnetic torque estimation $\hat{T}_e$ is computed from the estimated stator flux $\hat{\boldsymbol{\lambda}}_s$ and the measured stator current $\mathbf{i}_s$, where p is the number of pole pairs

$$\hat{T}_e = 3/2\, p\, (\hat{\lambda}_{s\alpha} i_{s\beta} - \hat{\lambda}_{s\beta} i_{s\alpha})\,. \tag{16}$$

IV. SPEED ESTIMATION

The mechanical-rotor position and speed mainly depend on the position (phase) of the rotor-flux vector $\hat{\boldsymbol{\lambda}}_r$. Two solutions are presented which extract the estimations of the

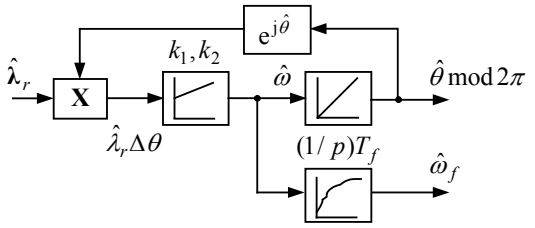

Fig. 2. PLL rotor speed estimator from rotor flux $\boldsymbol{\lambda}_r$.

rotor-flux position $\hat{\theta} = \hat{\theta}_r$ and the rotor-flux speed $\hat{\omega} = \hat{\theta}^{\bullet}$ from the estimated rotor flux $\hat{\boldsymbol{\lambda}}_r$. The mechanical variables are calculated to the end of this chapter.

A. Derivative Estimator

The speed ω is the derivative of the position θ, that is $\hat{\omega} = \hat{\theta}^{\bullet} = \text{atan}^{\bullet}(\hat{\lambda}_{r\beta} / \hat{\lambda}_{r\alpha})$ and thus [16]

$$\hat{\omega} = (\hat{\lambda}^{\bullet}_{r\beta}\hat{\lambda}_{r\alpha} - \hat{\lambda}^{\bullet}_{r\alpha}\hat{\lambda}_{r\beta}) / \hat{\lambda}_r^2, \quad \hat{\lambda}_r^2 = \hat{\lambda}_{r\alpha}^2 + \hat{\lambda}_{r\beta}^2 . \tag{17}$$

The same solution can be obtained on the other way taking into account that $\boldsymbol{\lambda}_r \perp \boldsymbol{\lambda}^{\bullet}_r$, i.e., orthogonal vectors. The speed $\hat{\omega}$ is achieved from imaginary part $\text{Im}(\boldsymbol{\lambda}^{\bullet}_r \boldsymbol{\lambda}^{\#}_r)$ where the superscript " # " refers to the conjugate operator. On the other hand, the real part $\text{Re}(\boldsymbol{\lambda}^{\bullet}_r \boldsymbol{\lambda}^{\#}_r) = 0$ leads to the orthogonal condition (18), not used in this approach.

$$\hat{\lambda}^{\bullet}_{r\alpha}\hat{\lambda}_{r\alpha} - \hat{\lambda}^{\bullet}_{r\beta}\hat{\lambda}_{r\beta} = 0 . \tag{18}$$

Equation (17) can be implemented in discrete-time using Euler method [8], [16] where the subscript "$_1$" denotes the variable delayed with one sampling period h.

$$\hat{\omega} = (\hat{\lambda}_{r\alpha 1}\hat{\lambda}_{r\beta} - \hat{\lambda}_{r\beta 1}\hat{\lambda}_{r\alpha}) / h\hat{\lambda}_r^2 . \tag{19}$$

The derivative estimation of the speed $\hat{\omega}$ (19) gives fast estimation and compact computation. However, estimation accuracy is based on the accuracy of rotor flux estimation $\hat{\boldsymbol{\lambda}}_r$ (11), (12) which depends on machine parameters. Moreover, the derivative methods are sensitive to noise via the measurement signals, i.e., the current vector $\mathbf{i}_s$.

B. PLL Estimator

The second solution to extract the estimation of rotor position $\hat{\theta}$ and speed $\hat{\omega}$ from the rotor flux vector $\hat{\boldsymbol{\lambda}}_r(\hat{\lambda}_{r\alpha}, \hat{\lambda}_{r\beta})$ uses an estimator based on phase locked-loop (PLL) technique. Only the phase $\hat{\theta}$ of $\hat{\boldsymbol{\lambda}}_r$ vector is required, the magnitude $\hat{\lambda}_r$ is not used. The PLL basic idea consists on: the phase estimation error $\Delta\theta = \hat{\theta} - \theta$ is obtained from the imaginary part $\text{Im}(\hat{\boldsymbol{\lambda}}_r \boldsymbol{\lambda}_1^{\#})$, where $\boldsymbol{\lambda}_1 = e^{j\hat{\theta}}$ is a unit vector.

$$\Delta\theta \approx (\hat{\lambda}_{r\beta}\cos\hat{\theta} - \hat{\lambda}_{r\alpha}\sin\hat{\theta}) / \lambda_r^* . \tag{20}$$

The speed and position estimator (Fig. 2) employ a state observer (21) that leads the PLL phase error $\Delta\theta$ (20) to zero. The position $\hat{\theta}$ uses the modulo 2π operator.

$$\begin{bmatrix} \hat{\theta} \\ \hat{\omega} \end{bmatrix}^{\bullet} = \begin{bmatrix} 0 & 1 \\ 0 & 0 \end{bmatrix} \begin{bmatrix} \hat{\theta} \\ \hat{\omega} \end{bmatrix} + \begin{bmatrix} k_1 \\ k_2 \end{bmatrix} \Delta\theta \tag{21}$$

To achieve a faster estimation convergence, a state and disturbance full-order Luenberger observer (22) based on the drive mechanical model can be used [12]. The main input is the estimated torque $\hat{T}_e$; the phase lag is reduced. The equivalent load torque $\hat{T}_L$ is the disturbance that really can be considered constant during a sampling period h.

$$\begin{bmatrix} \hat{\theta} \\ \hat{\omega} \\ \hat{T}_L \end{bmatrix}^{\bullet} = \begin{bmatrix} 0 & 1 & 0 \\ 0 & 0 & -1/J_o \\ 0 & 0 & 0 \end{bmatrix} \begin{bmatrix} \hat{\theta} \\ \hat{\omega} \\ \hat{T}_L \end{bmatrix} + \begin{bmatrix} 0 \\ 1/J_o \\ 0 \end{bmatrix} \hat{T}_e + \begin{bmatrix} k_1 \\ k_2 \\ k_3 \end{bmatrix} \Delta\theta , \tag{22}$$

where J_o is the equivalent mechanical inertia. The design of the correction gain matrix $[k_1, k_2, k_3]^{\text{T}}$ can use a pole allocation method. The observer poles are chosen as a compromise between fast estimation convergence and noise rejection.

C. Mechanical Speed Estimation

From the rotor-flux speed $\hat{\omega}$, estimated with one of the previous methods, the mechanical speed estimation $\hat{\omega}_m$ is given by:

$$\hat{\omega}_m = \hat{\omega} / p \qquad \text{for PMSM,} \tag{23}$$

$$\hat{\omega}_m = \hat{\omega} / p - \hat{\omega}_{sl} \qquad \text{for IM, with} \tag{24}$$

$$\hat{\omega}_{sl} = \frac{2\hat{R}_r}{3p}\frac{\hat{T}_e}{\hat{\lambda}_r^2}, \tag{25}$$

where $\hat{\omega}_{sl}$ – slip frequency, $\hat{R}_r$ – estimated rotor resistance (15), $\hat{\lambda}_r$ – estimated rotor-flux magnitude (12), or replaced by its reference value λ_r^*, p – pole pairs, $\hat{T}_e$ is given by (13).

The slip frequency (25) is mainly sensitive to rotor resistance identification $\hat{R}_r$ (15) depending on rotor temperature and this could be a problem at low speed.

V. Sensorless Direct Torque and Flux Control

A classical structure of the DTC with voltage-vector selection using a switching table [3] is applied for the sensorless control of PMSM drive [13] (Fig. 3).

The direct control of the VSI switches S_a, S_b, $S_c \in \{0,1\}$ selects the stator voltage discrete-vector from 8 vectors, i.e. $V_k = 2/3V_{dc}e^{j(k-1)\pi/3}$ for $k = 1,...,6$, or $V_k = 0$ for $k \in \{0,7\}$. The selection depends on three variables: θ_i ($i = 1,...,6$) – stator flux sector of $\pi/3$ radians that has the voltage vector V_i as bisector, τ – torque error, and ϕ – stator flux error. The torque controller is three-position hystheresis type (3H) with the output $\tau(1,0,-1)$. The flux controller is bi-position hystheresis type (2H) with the output $\phi(1,0)$. The associated actions at the controller outputs, corresponding with the values from brackets, are: for $\tau(1,0,-1)$ – increase, unmodified, decrease the motor torque T_e, and for $\phi(1,0)$ – increase, decrease the stator flux magnitude λ_s. The VSI table of optimal switching is given in Table I [3], [5]. This table can be implemented in a ROM memory with six bits for the input address: two bits for τ, one bit for ϕ, and three bits for θ_i; and three bits for the output data – the inverter switching states (S_a, S_b, S_c) which select the stator voltage discrete-vector $V_k (k = 0,...,7)$.

The stator flux sector $\theta_i (i = 1,...,6)$ can be obtained from the Table II that is based on sign comparisons using stator flux components $\hat{\boldsymbol{\lambda}}_s(\hat{\lambda}_{s\alpha}, \hat{\lambda}_{s\beta})$ [1].

The main part of the sensorless control is the observer that contains the improved flux estimator with DC-offset PI correction loop to estimate the stator flux vector $\hat{\boldsymbol{\lambda}}_s$ and the estimated motor torque $\hat{T}_e$ (Fig. 1) and the PLL estimator to estimate the speed $\hat{\omega}_f$ (Fig. 2).

TABLE I
TABLE OF OPTIMAL SWITCHING

θ_i – stator flux sector		τ – torque error 1	0	-1
ϕ – flux error	1	V_{i+1}	V_0, V_7	V_{i-1}
	0	V_{i+2}	V_0, V_7	V_{i-2}

TABLE II
STATOR FLUX SECTOR θ_i

$\text{sign}(\hat{\lambda}_{s\alpha})$	+	+	–	–	–	+
$\text{sign}(\hat{\lambda}_{s\beta})$		+	+		–	–
$\text{sign}(\sqrt{3}\lvert\hat{\lambda}_{s\beta}\rvert - \lvert\hat{\lambda}_{s\alpha}\rvert)$	–	+	+	–	+	+
θ_i	θ_1	θ_2	θ_3	θ_4	θ_5	θ_6

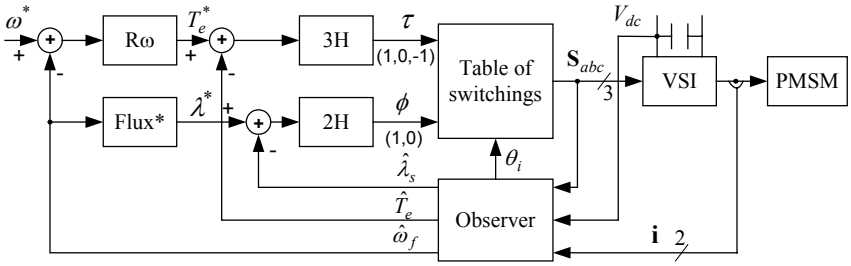

Fig. 3. Sensorless structure for classical DTC drive using the improved closed-loop integrator and PLL speed estimator.

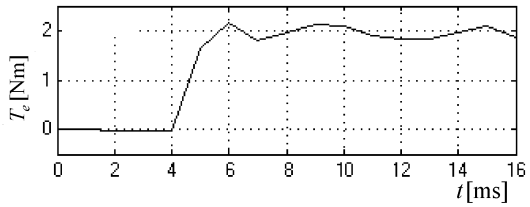

Fig. 4. Transient torque T_e, for reference torque $T_e^* = 2$ Nm step; very quick time response of 2 ms.

The speed controller (Rω) is a PI anti-windup type with first order low-pass filter (LPF1) on the speed reference ω^*. It is tuned after an extended symmetrical optimum criterion for the equivalent servo-system with DTC.

VI. SIMULATION RESULTS

Significant simulation results are selected to prove high-dynamic performances in wide speed range of the sensorless DTC of PMSM drive (Fig. 3), having the parameters given in Appendix.

The simulation uses Matlab-Simulink package with simple Euler method. The sampling rate is $h = 100\,\mu s$ according to typical IGBT inverters. The scenarios take into account the following aspects.

Fig. 4 presents the torque response for a step rated torque reference applied at 4 ms. The torque time response is very quickly of 2 ms - specifically in DTC, with acceptable chattering in steady state operation.

Figs. 5 to 7 show high-dynamic performances in wide speed range operation (10-1000 rpm) step reversal, for zero to rated load-torque, with specified disturbances. The selected transient responses are: ω, $\hat{\omega}$ – real and estimated mechanical speed, T_e – electromagnetic torque, λ – stator flux magnitude, $\hat{\mathbf{e}}_{dc}(\hat{e}_{dc\alpha}, \hat{e}_{dc\beta})$ – components of DC-drift vector estimation, $\theta - \hat{\theta}$ – electric rotor position error.

Fig. 5 proves the correct estimation and compensation of the input DC-drift vector $\mathbf{e}_{dc}^*$ and high-dynamics at very low speed step reversal ±10 rpm, for zero to rated load-torque. The scenario consist of: 1) at $t = 0$ s, step DC-drift vector $\mathbf{e}_{dc}^* = -0.05 + j\,0.05$ and step speed $\omega^* = -10$ rpm, 2) at $t = 3$ s, reversal step speed $\omega^* = 10$ rpm, 3) at $t = 4$ s, rated load-torque step $T_L^* = 2$ Nm.

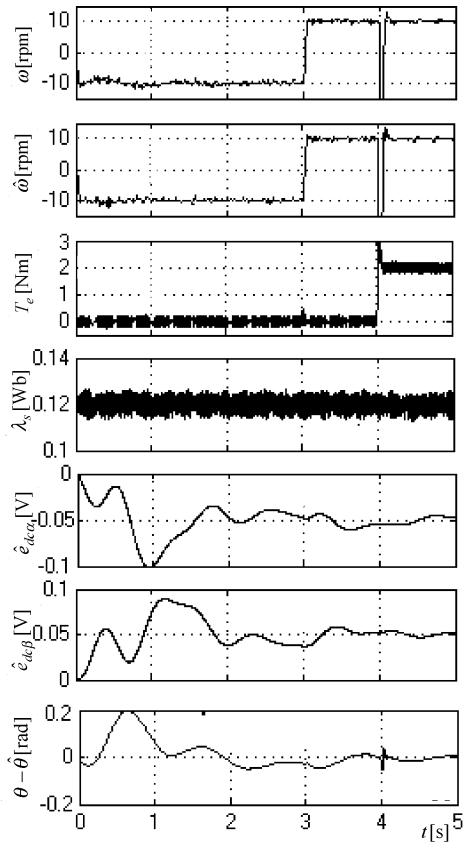

Fig. 5. High dynamic with offset compensation at very low speed step reversal $\omega^* = \pm 10$ rpm, rated load-torque step $T_L^* = 2$ Nm, with input drift vector $\mathbf{e}_{dc}^* = -0.05 + j\,0.05$.

The DC-drift vector estimation $\hat{\mathbf{e}}_{dc}$ converges to $\mathbf{e}_{dc}^*$ and compensates the DC-offset in the flux estimation λ. The position error converges to zero and practically does not depend on load-torque even at step applied. The transient speed estimation has a good accuracy with low ripple in steady state. On the other hand, when step rated load-torque is applied, a relative sharp-drop speed appears because the speed controller is not so fast (frequency bandwidth).

Fig. 6 proves the cancellation of the flux error due to inaccurate identification of the stator resistance R_s with +10%, and high-dynamics at low speed step reversal ±20 rpm, for zero to half-rated step load-torque.

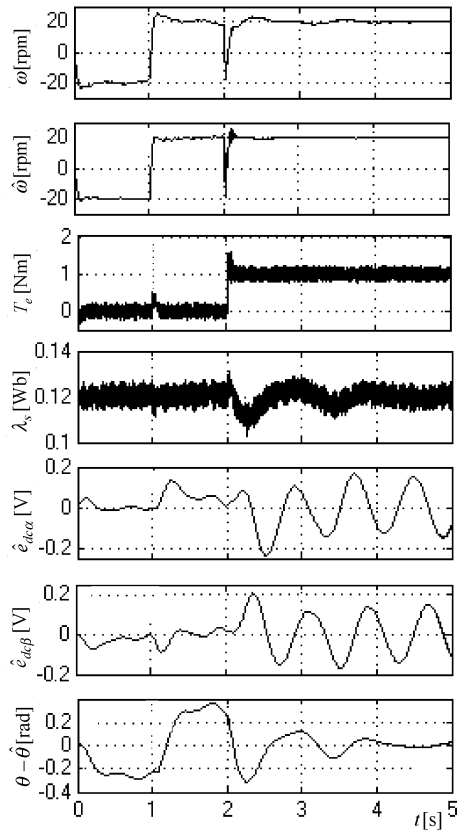

Fig. 6. High dynamic and robustness to R_s detuning at very low speed step reversal $\omega^* = \pm 20$ rpm, load-torque step $T_L^* = 1$ Nm, with stator resistance error $R_s = 1.1R_{so}$.

The scenario consists of: 1) at $t = 0$ s, step speed $\omega^* = -20$ rpm, 2) at $t = 1$ s, reversal step speed $\omega^* = 20$ rpm, 3) at $t = 2$ s, step load-torque $T_L^* = 1$ Nm. In the first stage (no loaded motor), the DC-drift estimation $\hat{\mathbf{e}}_{dc}$ converges to zero because the voltage drop $R_s\mathbf{i}_s$ goes to zero. In the second stage (loaded motor), a harmonic error $\Delta R_s\mathbf{i}_s$ is present at the integrator input, and a harmonic correction vector $\hat{\mathbf{e}}_{dc} \to \Delta R_s\mathbf{i}_s$ with stable magnitude compensates this parameter disturbance. After the transient operation, the stator flux magnitude λ converges to the reference flux λ^*, and the rotor position (rotor flux angle) error $\theta - \hat{\theta}$ converges to zero. These significant results prove the effective robustness of the proposed solution regarding $\hat{R}_s$ identification error.

The chattering in the electromagnetic torque from Figs. 4 to 6 ($h = 0.1$ ms) could be reduced using a shorter sample rate h with faster DSP controller and faster IGBT.

Note: Referring to Fig. 1, the flux $\hat{\boldsymbol{\lambda}}_s$ is correctly estimated while the flux $\hat{\boldsymbol{\lambda}}$ at the integrator output is rising in magnitude to compensate $\Delta R_s\mathbf{i}_s$ error. The key procedure is based on the fact that parameter errors determine mainly magnitude flux estimation $\hat{\lambda}$ error, but rather minor phase estimation $\hat{\theta}$ error [9]–[11]; this is the case of $\hat{\boldsymbol{\lambda}}$. The convergence of the rotor-flux angle in presence of the stator resistance error (Fig. 6) proves the idea (13) to correct the flux magnitude in the design conditions (10).

Fig. 7 proves high-dynamic performances at high-speed step reversal ±1000 rpm, for zero to rated load-torque step. The scenario consist on: 1) at $t = 0$ s, step speed $\omega^* = -1000$ rpm, 2) at $t = 0.3$ s, reversal step speed $\omega^* = 1000$ rpm, 3) at $t = 0.7$ s, rated load-torque step

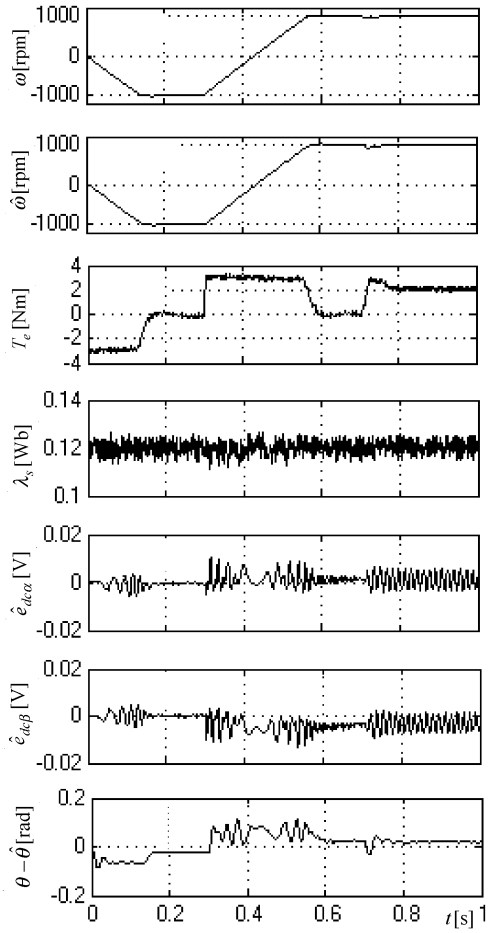

Fig. 7. High dynamic at high-speed step reversal $\omega^* = \pm 1000$ rpm with rated load-torque step $T_L^* = 2$ Nm.

$T_L^* = 2$ Nm. The speed, torque and flux present good dynamic responses.

VII. Experimental Results

For technical reasons, and also to prove the universality of the proposed estimation technique, a sensorless DTC for IM with parameters given in Appendix was investigated.

The IM sensorless structure is similarly as in Fig. 3, but the VSI is controlled by space vector modulation (SVM).

The experimental setup contains the elements [8]:
- dual processor system: ADSP-21062 general purpose DSP and ADMCF328 motor controller DSP,
- analog interface to measure two phase currents and the V_{dc} link voltage,
- speed encoder (5000 lines) only for speed monitoring,
- DC machine mechanical connected to IM, as load.

The estimator structure for all estimated variables used in sensorless DTC of IM is summarized in Fig. 8. A real-time identification algorithm estimates the stator resistance $\hat{R}_s$.

Fig. 9 presents the experimental results at low speed - step reversal $\omega^* = \pm 30$ rpm, at full load. The scenarios consist of: 1) $t = 0 \sim 2.3$ s, $\omega^* = 30$ rpm, steady state, 2) $t_2 = 2.3$ s, reversal step speed $\omega^* = -30$ rpm.

These results prove good performance of sensorless DTC of IM drive in steady state and transient regimes at low- speed, with good speed estimation and fast speed and torque response. The stator and rotor flux magnitude is practically constant.

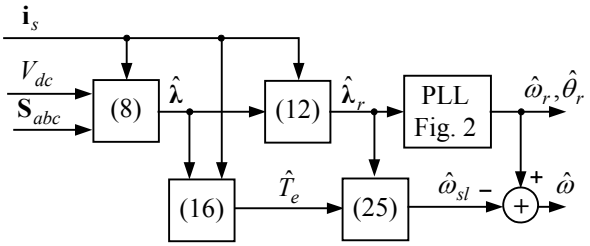

Fig. 8. Estimator for $\hat{\boldsymbol{\lambda}}$, $\hat{\boldsymbol{\lambda}}_r$, $\hat{T}_e$ and $\hat{\omega}$ in sensorless DTC of IM drive. Numbers in brackets represent the relevant equations.

Fig. 10 presents the experimental results, from startup, without initial flux installed, to step high-speed $\omega^* = 1500$ rpm.

The speed, torque and flux responses are good. The speed response is long because the torque is in limitation (12 Nm) and equivalent rotor inertia is big ($J_{ech} = 0.08\,\text{kgm}^2$). The torque ripple at high-speed steady state is given by the poor technical nature of the DC-generator as load. The stator flux is quickly installed at startup. There is a small error in steady state.

VIII. CONCLUSIONS

The main conclusions and contributions are as following.

- A robust flux-linkage estimator with high-dynamic accuracy in wide speed range is developed for all AC drives with sinusoidal flux distribution, including sensorless control.
- The flux-linkage estimator is based on an improved integrator using voltage model in stator reference with a DC-offset PI-correction loop that operates with the reference flux magnitude in the correction error.
- The DC-drift vector estimation is memorized by the PI integral component and DC-offset is totally canceled; thus, the equivalent flux estimator works as a pure integrator with zero-lag and high-dynamic accuracy.
- The stator resistance identification error affects the flux estimation at the integrator output mainly in magnitude, but rather plays a minor role in phase estimation error.
- A phase locked loop is used as state estimator to extract the speed / position from the estimated rotor flux vector.
- A sensorless DTC for PMSM drive is investigated by simulation using this estimation technique. Extensive simulation results prove high-dynamic performances and estimation robustness in large speed range step reversal: ±10 rpm, ±1000 rpm, for zero to rated load-torque step. They highlight input DC-drift cancellation, initial-flux error cancellation, and robust flux, speed/ position estimation to stator resistance identification errors.
- The experimental results for a sensorless DTC for IM drive with space vector modulation and using the same estimation technique prove good transient and steady state performances in large speed range 30-1500 rpm, at step speed references.

APPENDIX

1) Parameters of the Sensorless DTC of PMSM Drive

PMSM rated data: $I_a = 3$ A, $T_e = 2$ Nm, $\omega_m = 1000$ rpm,

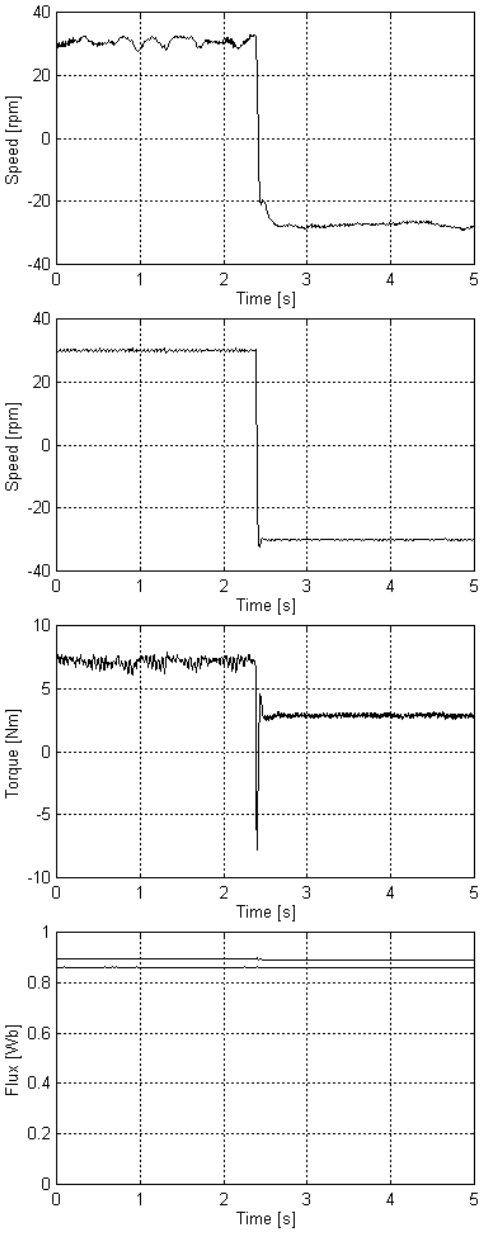

Fig. 9. Experimental results at low speed step reversal $\omega^* = \pm 30$ rpm, full loaded: measured mechanical speed ω, estimated mechanical speed $\hat{\omega}$, estimated electromagnetic torque $\hat{T}_e$, estimated stator flux $\hat{\lambda}_s$ (upper trace) and estimated rotor flux $\hat{\lambda}_r$ (lower trace).

$V_{dc} = 100$ V, parameters: $J = 0.004\,\text{kgm}^2$, $R_s = 1.8$ Ohm, $B = 0.001$ Nms/rad, $p = 4$, $\lambda_{PM} = 0.1$ Wb, $L = 0.02$ H.

- DTC: $\lambda^* = 1.2\lambda_{PM}$, $\Delta T_e = 0.04 T_e$, $\Delta\lambda = 0.02\lambda^*$, $h = 100$ μs.
- Rω - speed controller PI anti-windup with ω^* LPF1: $k_{pw} = 0.25$, $T_{iw} = 0.03$ s, $T^*_{fw} = 0.03$ s, $k_{aw} = 10$, $T_{eLim} = 3$.
- Flux estimator (Fig. 1): $k_p = 3$, $k_i = 10$, $\hat{R}_s = R_s$, $L_o = L$.
- Speed and position PLL estimator (Fig. 2): $k_1 = 100$, $k_2 = 50000$, $T_f = 4$ ms, $L_o = L$.

2) Parameters of the Sensorless DTC of IM Drive

- IM rated data: $P = 1.1$ kW, $U_s = 380$ V, $f_s = 50$ Hz, $T_e = 7$ Nm; parameters: $R_s = 5.46$ Ohm, $R_r = 4.45$ Ohm, $J = 0.008\,\text{kgm}^2$, $J_{\text{Load}} = 0.07\,\text{kgm}^2$, $L_s = L_r = 0.492$ H, $L_m = 0.475$ H $p = 2$.
- VSI: $P = 4.3$ kVA, type VLT5004 Danfoss.

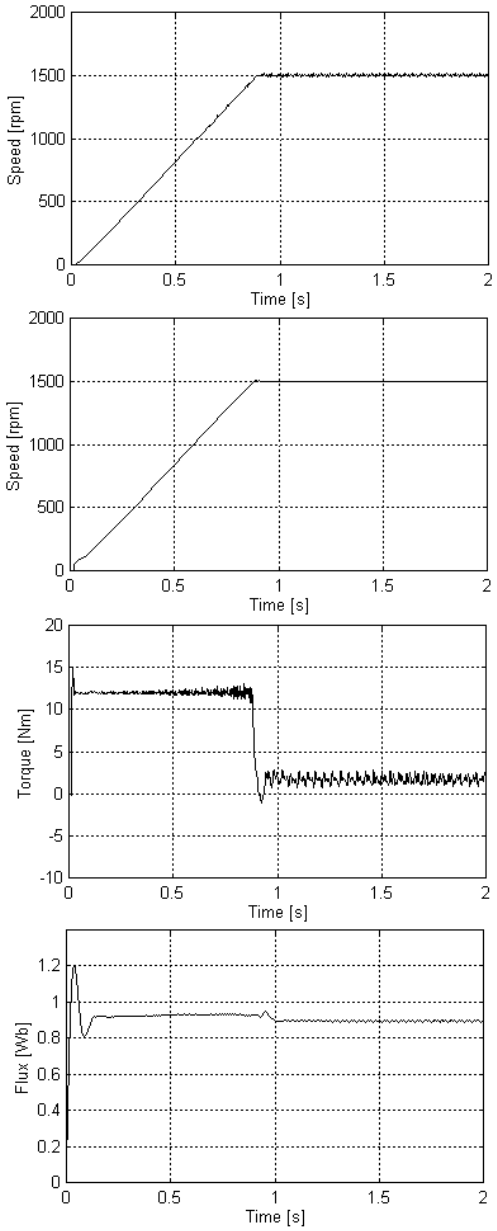

Fig. 10. Experimental results at high speed step $\omega^* = 0 \sim 1500$ rpm: measured mechanical speed ω, estimated mechanical speed $\hat{\omega}$, estimated electromagnetic torque $\hat{T}_e$, estimated stator flux $\hat{\lambda}_s$ (no initial flux installed).

ACKNOWLEDGMENT

The authors would like to thank Dr. Cristian Lascu from Politehnica University of Timisoara for his valuable work helping us in the experimental results.

REFERENCES

[1] I. Boldea and S. A. Nasar, *Vector Control of AC Drives*. CRC Press, Boca Raton, Florida, 1992.

[2] P. Vas, *Sensorless Vector and Direct Torque Control*. Oxford University Press, 1998.

[3] I. Takahashi and T. Noguchi, "A new quick-response and high-efficiency control strategy of an induction motor," *IEEE Trans. Ind. Applicat.*, vol. 22, no. 5, pp. 820-827, Sep./Oct. 1986.

[4] J. N. Nash, "Direct torque control, induction motor vector control without an encoder," *IEEE Trans. Ind. Applicat.*, vol. 33, no. 2, pp 333-341, Mar./Apr. 1997.

[5] J. -K. Kang and S. -K. Sul, "New direct torque control of induction motor for minimum torque ripple and constant switching frequency," *IEEE Trans. Ind. Applicat.*, vol. 35, no. 5, pp. 1076-1082, Sep./Oct. 1999.

[6] T. G. Habetler, F. Profumo, M. Pastorelli, and L. M. Tolbert, "Direct torque control of induction machines using space vector modulation," *IEEE Trans. Ind. Applicat.*, vol. 28, no. 5, pp. 1045-1052, Sep./Oct. 1992.

[7] D. Casadei, G. Serra, A. Tani, L. Zarri, and F. Profumo, "Performance analysis of a speed sensorless induction motor drive based on constant switching frequency DTC scheme," in *Proc. IEEE-IAS 2000*, vol. 3, pp. 1360-1367, 2000.

[8] C. Lascu and I. Boldea, "Direct torque control of sensorless induction motor drives. A sliding mode approach," in *Proc. OPTIM 2002*, Brasov, vol. 2, pp. 481-488, 2002.

[9] G. D. Andreescu, "Flux-estimator with offset correction loop for low speed sensorless control of AC drives," in *Proc. OPTIM 2002*, Brasov, vol. 2, pp. 531-538, 2002.

[10] P. L. Jansen, R. D. Lorenz, and D. W. Novotny, "Observer-based direct field orientation: Analysis and comparison of alternative methods," *IEEE Trans. Ind. Applicat.*, vol. 30, no. 4, pp. 945-953, Jul./Aug. 1994.

[11] D. E. Borgard, G. Olsson, and R. D. Lorenz, "Accuracy issues for parameter estimation of field oriented induction machine drives," *IEEE Trans. Ind. Applicat.*, vol. 31, no. 4, pp. 795-801, Jul./Aug. 1995.

[12] R. D. Lorenz, "Observers and state filters in drives and power electronics," in *Proc. OPTIM 2002*, Brasov, Keynote pp. XIX-XXVIII, 2002.

[13] G. D. Andreescu, "Flux observers based on combined voltage-current models for control of PMSM," in *Proc. EPE-PEMC 2000*, Kosice, vol. 6, pp. 64-69, 2000.

[14] J. Holtz and J. Quan, "Sensorless vector control of induction motors at very low speed using a nonlinear inverter model and parameter identification," in *Proc. IEEE-IAS 2001*, vol. 4, pp. 2614-2621, Chicago, 2001.

[15] H. Kubota, K. Matsuse, and T. Nakano, "DSP-based speed adaptive flux observer of induction motor," *IEEE Trans. Ind. Applicat.*, vol. 29, no. 2, pp. 344-348, Mar./Apr. 1993.

[16] M. Rodnic and K. Jezernik, "An analysis of speed sensorless torque and flux controller for induction motor," in *Proc. PESC 2000*, Galway, vol. 2, pp. 867-872, 2000.

[17] D. Casadei, G. Serra, and A. Tani, "Stator flux vector control of induction motors using a new closed-loop flux estimator," in *Proc. PEMC 1998*, vol. 3, pp. 85-90, Prague, 1998.

[18] B. K. Bose and N. R. Patel "A programmable cascaded low-pass filter-based flux synthesis for stator flux-oriented vector-controlled induction motor," *IEEE Trans. on Ind. Electron.*, vol. 44, no. 1, pp. 140-143, Jan./Feb. 1997.

[19] J. Hu and B. Wu, "New integration algorithms for estimating motor flux over a wide speed range," *IEEE Trans. Power Electron.*, vol. 13, no.5, pp. 969-977, Sep. 1998.

Gheorghe Daniel Andreescu received the M.Sc. degree in applied electronics in 1977 and Dr.Sci. degree in control engineering in 1999, both from the Politehnica University of Timisoara (PUT), Romania.

From 1977 to 1984, he was employed as a Research Engineer at the Electrotimis company Timisoara. In 1984, he joined the Automation and Industrial Informatics (AII) Department of PUT, and became Associate Professor in 2000. From 1993 he is also with TIMTEH Electronics Ltd., Timisoara working in automatic testing for avionics, e.g., for British Airways Avionics Engineering. His research interests include sensorless control of electrical drives, observers, real time implementations, automatic testing, monitoring and control of distributed systems.

Dr. Andreescu is a member of the IEEE: Industry Application Society, Robotics and Automation Society, the Romanian Association in Robotics the Romanian Society of Control Engineers and Technical Informatics.

Adrian Popa received the B.Sc. and M.Sc. degrees in control engineering from PUT, Romania, in 1996 and 1997, respectively.

From 1996 to 1998, he was employed as a research engineer at the Institute for Computers Bucharest, Romania. In 1998, he joined the AII Department of PUT, as an Assistant Professor. Since 2000, he is with Siemens VDO Automotive, where he is now group leader at the Software Department, Powertrain division at the site of Timisoara.

His research interests include real time systems, embedded systems, with application in PMSM sensorless control and control of Diesel engines.

Mr. Popa is a member of the Romanian Society of Control Engineers and Technical Informatics.